



MHD thermogravitational heat transfer within complex enclosure considering the influence of different wavy patterns

Ammar Abdulkadhim^{1,2} · Isam Mejbel Abed¹ · Nejla Mahjoub Said^{3,4}

Received: 4 January 2022 / Accepted: 13 July 2022 / Published online: 21 August 2022
© Akadémiai Kiadó, Budapest, Hungary 2022

Abstract

The present work examines utilizing CFD simulation of the natural convection within complex enclosure with four different cases of wavy patterns considering the existence of inner heated elliptical body. The influence of inclined magnetic field had been taken into consideration. The space between the inner body and the enclosure had been filled by two layers. The first right layer was filled by nanofluid while the second left layer had been filled by porous medium with the same nanofluid. The influence of various parameters such as number of undulations, the distance between the wavy walls, and the inner elliptical body position for four different cases of wavy walls patterns with and without magnetic field on fluid flow and heat transfer had been drawn in terms of streamlines, isotherms and Nusselt number. The results indicate that in the absence of magnetic field the Case 3 has the highest stream function with a dimensionless value of $|\Psi_{\max}| = 34.229$ which make Case 3 is recommended wavy patterns for bettering the fluid flow strength when the number of undulations kept at ($N = 1$) and the distance between the wavy walls kept at ($B = 0.8$). It is important to note that at ($B = 0.8$), Case 1 has the lowest strength of the fluid flow while it enhanced by 41.17% when ($B = 1.0$). On the other hand, increasing the distance between wavy walls from ($B = 0.8$) into ($B = 1.4$) enhances Nusselt number by 31.67%. The influence of inner body position had the highest impact of heat transfer rate in a comparison with the other as it helps in improvement of Nusselt number by 67.70% when it moves toward to bottom of the enclosure. Generally, the magnetic field reduces both of the fluid flow intensity and heat transfer for all of the shape of wavy patterns.

Keywords Natural convection · Nanofluid · Porous medium · MHD · Wavy · Elliptical

Introduction

The study of buoyancy driven flow which formally known as natural convection within enclosures considering different geometrical shapes had been studied a lot due to their outstanding applications related to energy consumption and conversion such as food processing [1] sustainable building

[2], solar air heaters [3], different shapes of solar collectors [4–7], materials processing [8], chemical reactions [9], cooling systems of nuclear chemical reactor [10–12], heat exchangers [13, 14], etc. Many of previous works were presented to study the phenomenon of natural convection within different shape of enclosures such as square [15–17], rectangular [18–20], triangular [21], trapezoidal [22–24], rhombus [25], circular [26], parallelogrammic [27], elliptical [28, 29], wavy [30] utilizing different numerical method such as finite difference, finite element and finite volume formulation. Based upon the previous publications, there is abundant in the studies regarding the simple shapes while there is gap regarding the more complex shapes such as wavy-shaped enclosure.

Some of the studies of natural convection within simple shapes of enclosures had been presented by numerous researchers. The convection within square enclosure had been investigated by Goodarzi et al. [31, 32]. Also, MHD effect on natural convection within square enclosure had

✉ Nejla Mahjoub Said
nejla.mahjoub@fsm.rnu.tn; nalmahjoub@kku.edu.sa

¹ Mechanical Engineering Department, University of Babylon, Hillah, Babylon Province, Iraq

² Air Conditioning and Refrigeration Techniques Engineering Department, Al-Mustaqbal University College, Hillah, Babylon Province, Iraq

³ Department of Physics, College of Science, King Khalid University, Abha 61413, Saudi Arabia

⁴ LGM, Preparatory Institute for Engineering Studies, University of Monastir, 5000 Monastir, Tunisia

been studied by Pordanjani et al. [33] using FORTRAN code based upon finite volume method. Goodarzi et al. [34] used finite volume formulation to study the influence of Rayleigh number along with the geometric aspect ratio on natural convection heat transfer as well as the entropy generation within nanofluid filled rectangular enclosure.

The multi-layers systems had been taken a lot of attention and studied recently by various researchers. Mehryan et al. [35] used finite element method to study the natural convection within a square enclosure filled by solid layer, porous medium layer in addition to the third nanofluid layer considering thermal non-equilibrium model. Hussain and Rahomey [36] studied the natural convection within square enclosure considering different inner bodies (circle, elliptical, triangular, rhombus and rectangular). The space between them and been filled by nanofluid in the right layer with porous medium saturated with the same nanofluid in the left layer.

The wavy enclosure had been studied by many researchers that used finite volume formulation considering the existence of internal heat generation [37]. The influence of wavy patterns on heat transfer in addition to the entropy generation of Cu-water nanofluid enclosure had been investigated via finite volume formulation by [38, 39]. The results showed that entropy generation and Nusselt number reduces with increasing of nanofluid loading. Also, the influence of different types of nanofluid such as TiO_2 -water, Cu-water and Al_2O_3 -water on heat transfer thermal rate and the generation of entropy within complex wavy enclosure that had been simulated numerically using formulation based upon finite volume scheme [40]. The finite difference scheme used to study the natural convection as well as entropy generation in triangular-wavy porous enclosure under wide range of Darcy number in addition to Rayleigh number along with number of undulations [41]. The undulation increases the entropy generation in a comparison with that of without undulations. The influence of inclined magnetic field on inclined square-wavy enclosure filled by nanofluid considering heater in the corner had been investigated by Sheremet et al. [42] utilizing finite difference methodology. The CVFEM used to study the influence of magnetic field on complex wavy enclosure filled by Fe_3O_4 -water nanofluid under wide range of dimensionless numbers such as Hartmann and Rayleigh numbers, nanofluid loading in addition to the amplitude of sinusoidal wall [43]. Finite difference method had been used by Reference [44] to examine the natural convection within wavy enclosure heated partially from its left sidewall and filled by nanofluid and porous medium. Alrowaili et al. [45] studied the natural convection in MHD wavy enclosure considering three different wavy walls (Out-Out, In-In, In-Out) surfaces using finite element method. The results showed that In-In wavy pattern reveals the lowest convection transport.

The existence of inner body within wavy enclosure had been received attention by Nemours researchers considering

the influence of the shape of inner bodies, their size and position. Many researchers used finite element method in this specific subject to examine the influence of inner cylindrical body size on natural convection within wavy enclosure [46]. The results indicate that there is a critical value of inner cylinder diameter which if it increases beyond this value, a reduction in heat transfer will be noted. Also, a comparison between the wavy and circular enclosure had been done which leads to prove that the wavy shape reveals better heat transfer rate more than the circular shape. The influence of inner rotating solid cylinder immersed in a porous wavy enclosure heated partially studied from its bottom wall had been studied by Alsabery et al. [47]. The magnetic field on natural convection between circular cylinder in a wavy enclosure had been demonstrated by [48, 49]. The inner wavy body had been studied within wavy enclosure had been studied by [50, 51]. For example, Abdulkadhim et al. [51] studied the inner wavy body on natural convection within a nanofluid-porous wavy enclosure using local thermal equilibrium model. In another study where local thermal non-equilibrium model had been utilized to study the natural convection between inner cylindrical body immersed in a nanofluid-porous wavy enclosure [52]. Also, Dogonchi and Hashim [53] studied the natural convection within wavy enclosure filled by nanofluid considering the existence of inner rhombus body using CVFEM to examine the impact of inner body. It was obtained that for better heat transfer, the decreasing of the size of inner body is recommended. The inner square enclosure within wavy enclosure had been reported by [54]. The elliptical inner body within wavy enclosure under the influence of magnetic field had been examined by [55] by finite element method. The space had been filled by nanofluid and porous medium. Darcy–Forchheimer model had been used for treating the porous medium. Ganesh et al. [56] studied the fluid flow considering fins and inner circular body in a wavy enclosure filled by MWCNT and proposed new correlations of Nusselt number. Mourad et al. [57] studied the MHD free convection as well as entropy generation between Koch Snowflake located inside wavy enclosure filled by nanofluid and porous medium.

Recently, more attention had been given to the complex shapes of enclosure like U-shape [58], I-shaped [59], F-shape [60], E-shape [61]. For example, [62] used lattice Boltzmann scheme to study the magnetic field on natural convection within incinerator enclosure considering the inner hot block body.

As indicated above, these results had the application within the study of heat transfer in a shell and tube heat exchanger in industrial systems. Also, the Darcy–Brinkman model had been used for the modeling of fluid flow saturated with porous medium started by Darcy model. After that, two extensions of Darcy model had been proposed. The first model was due to Forchheimer that used for moderate

and high Reynolds number by addition of nonlinear term to Darcy model. Unfortunately, this model still not able to predict the flow through high porosity and confined media. The second extension was introduced to Darcy model by Brinkman, which included a second-order viscous term with an equivalent viscosity for the porous medium. This modification allows the use of no-slip conditions on confining walls and gives accurate results at higher porosity values.

It can be seen that there are serious limitations on the combined enclosures which they are a combination of more than single enclosure. This case is the most case that closes to the real industrial applications. Besides, there are limitations in the I-shape enclosure studies in spite its applications in shell and tube heat exchangers thermal systems in the industrial applications [59, 63–68]. So, it can be seen that there is no published study focuses on studying of the natural convection within I-shaped along with wavy-walled enclosure with the existence of inner elliptical body considering the influence of four cases of different wavy patterns under inclined magnetic field when the enclosure filled by nanofluid and porous medium. In this way, the objective of the present work is to illustrate the influence of the wavy patterns under four different cases (In-In, In-Out, Out-In, Out-Out), magnetic field, distance between the wavy walls,

number of undulations and position of the inner body on the fluid flow intensity along with the heat transfer.

Mathematical model

The natural convection in an I-shaped wavy enclosure filled by nanofluid in the right layer along with porous medium saturated with the same nanofluid in the left layer considering the existence of inner elliptical body had been solved via finite element method. Darcy–Brinkman model had been used to model the porous media considering the local thermal equilibrium approach between nanofluid and porous medium. The inclined magnetic field had been applied to show its impact on fluid flow and heat transfer. Four different cases of wavy patterns which they are (Case 1: In-In, Case 2: In-Out, Case 3: Out-In, Case 4: Out-Out) to show their impact on fluid flow and heat transfer will studied had been discussed in Fig. 1. The assumptions had been listed below:

- The fluid flow is laminar along with incompressible under steady and two-dimensional

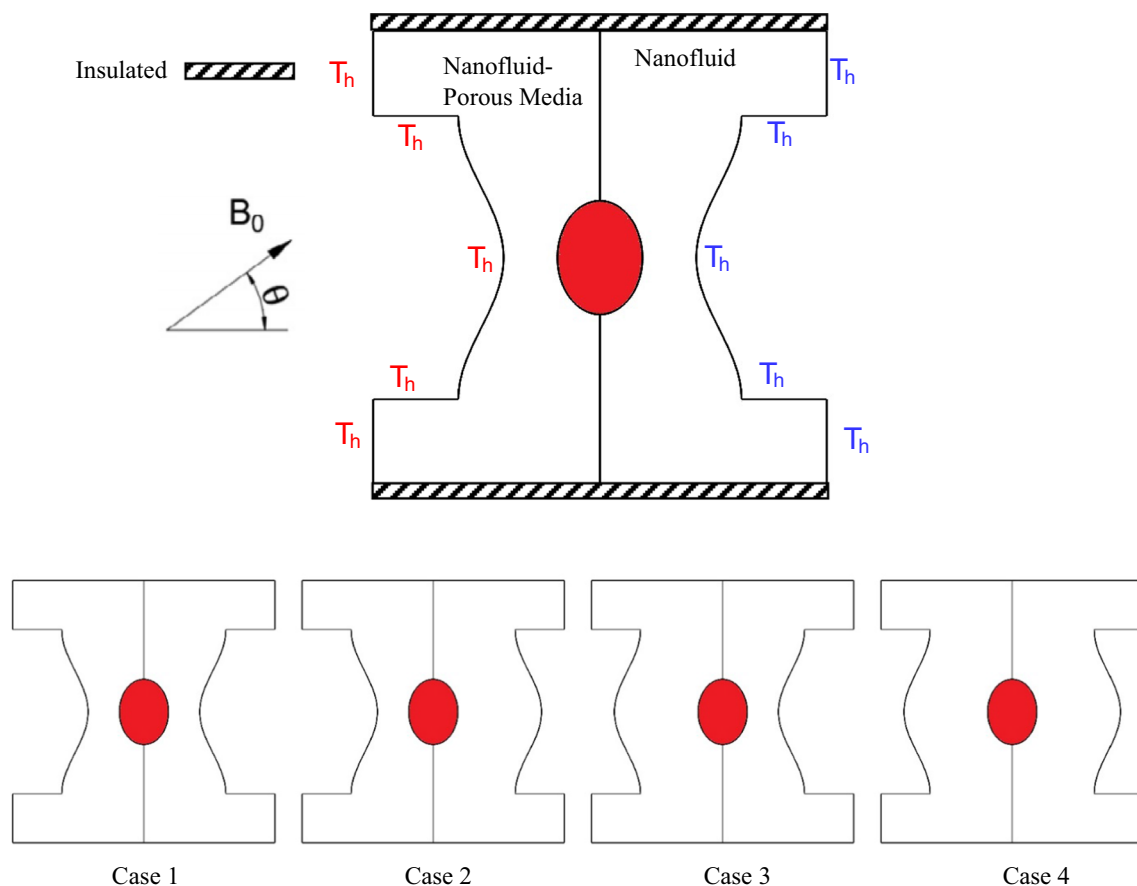


Fig. 1 The physical model and the selected CFD cases of the present problem

- No slip conditions had been applied to all of the elliptical as well as the walls of the enclosure while the interface wall which separates the left and right layer had been considered to be permeable.
- Local thermal equilibrium model had been applied between the porous medium and nanofluid
- Darcy-Brinkman had been used to predict the fluid flow within the porous medium
- Constant nanofluid thermophysical properties while Boussinesq approximation had been considered to treat the density in the body force of momentum equation

The governing equations for the present multi-layers systems had been written below in the dimensionless form for

$$U \frac{\partial V}{\partial X} + V \frac{\partial V}{\partial Y} = -\epsilon^2 \frac{\partial P}{\partial Y} + \epsilon \frac{\mu_{nf}}{\rho_{nf}\alpha_f} \left(\frac{\partial^2 V}{\partial X^2} + \frac{\partial^2 V}{\partial Y^2} \right) - \epsilon^2 \frac{\mu_{nf}}{\rho_{nf}\alpha_f} \frac{V}{Da} + \epsilon^2 \frac{(\rho\beta)_{nf}}{\rho_f\beta_{nf}} Ra\theta + \epsilon^2 Ha^2 PrV (U \sin(\gamma) \cos(\gamma) - V \cos^2(\gamma)). \tag{7}$$

each layer:

- **For right region (nanofluid layer):**

Continuity

$$\frac{\partial U}{\partial X} + \frac{\partial V}{\partial Y} = 0 \tag{1}$$

X – momentum

$$U \frac{\partial U}{\partial X} + V \frac{\partial U}{\partial Y} = -\frac{\partial P}{\partial X} + \frac{\mu_{nf}}{\rho_{nf}\alpha_f} \left(\frac{\partial^2 U}{\partial X^2} + \frac{\partial^2 U}{\partial Y^2} \right) + PrHa^2 (V \sin(\gamma) \cos(\gamma) - U \sin^2(\gamma)) \tag{2}$$

Y – momentum

$$U \frac{\partial V}{\partial X} + V \frac{\partial V}{\partial Y} = -\frac{\partial P}{\partial Y} + \frac{\mu_{nf}}{\rho_{nf}\alpha_f} \left(\frac{\partial^2 V}{\partial X^2} + \frac{\partial^2 V}{\partial Y^2} \right) + \frac{(\rho\beta)_{nf}}{\rho_f\beta_{nf}} Ra\theta + Ha^2 PrV (U \sin(\gamma) \cos(\gamma) - V \cos^2(\gamma)). \tag{3}$$

Energy

$$U \frac{\partial \theta}{\partial X} + V \frac{\partial \theta}{\partial Y} = \frac{\alpha_{nf}}{\alpha_f} \left(\frac{\partial^2 \theta}{\partial X^2} + \frac{\partial^2 \theta}{\partial Y^2} \right). \tag{4}$$

- **For left layer (Nanofluid-Porous medium layer):**

Continuity

$$\frac{\partial U}{\partial X} + \frac{\partial V}{\partial Y} = 0. \tag{5}$$

X – momentum

$$U \frac{\partial U}{\partial X} + V \frac{\partial U}{\partial Y} = -\epsilon^2 \frac{\partial P}{\partial X} + \epsilon \frac{\mu_{nf}}{\rho_{nf}\alpha_f} \left(\frac{\partial^2 U}{\partial X^2} + \frac{\partial^2 U}{\partial Y^2} \right) - \epsilon^2 \frac{\mu_{nf}}{\rho_{nf}\alpha_f} \frac{U}{Da} + PrHa^2 (V \sin(\gamma) \cos(\gamma) - U \sin^2(\gamma)) \tag{6}$$

Y – momentum

Energy

$$U \frac{\partial \theta}{\partial X} + V \frac{\partial \theta}{\partial Y} = \frac{\alpha_{eff}}{\alpha_f} \left(\frac{\partial^2 \theta}{\partial X^2} + \frac{\partial^2 \theta}{\partial Y^2} \right) \tag{8}$$

The thermo-physical properties of the nanoparticle and water had been inserted in Table 1. Additionally, the following formula for determination the properties of nanofluid [69]:

$$\alpha_{na} = \frac{k_{na}}{(\rho c_p)_{nf}} \tag{9}$$

$$\rho_{na} = (1 - \phi)\rho_{bf} + \phi\rho_{sp} \tag{10}$$

$$\rho c_p = (1 - \phi)(\rho c_p)_{bf} + \phi(\rho c_p)_{sp} \tag{11}$$

$$(\rho\beta)_{na} = (1 - \phi)(\rho\beta)_{bf} + \phi(\rho\beta)_{sp} \tag{12}$$

The correlations for determination of dynamics viscosity and thermal conductivity are based upon [70–73]:

Table 1 Thermophysical properties of nanofluid [75]

Properties	$\rho/\text{kg m}^{-3}$	$C_p/\text{J kg}^{-1} \text{K}^{-1}$	$k/\text{W m}^{-1} \text{K}^{-1}$	βK^{-1}
Water	997	4180	0.614	$2.1 \cdot 10^{-4}$
Al_2O_3	3970	765	40	$0.85 \cdot 10^{-5}$

$$\mu_{na} = \frac{\mu_{bf}}{(1 - \phi)^{2.5}} \tag{13}$$

$$\frac{k_{na}}{k_{bf}} = \frac{k_{sp} + 2k_{bf} - 2\phi(k_{bf} - k_{sp})}{k_{sp} + 2k_{bf} + 2\phi(k_{bf} - k_{sp})} \tag{14}$$

The effective thermal conductivity as well as the coefficient of thermal diffusion can be obtained as indicated below:

$$k_{eff} = (1 - \epsilon)k_{sp} + \epsilon k_{na} \tag{15}$$

$$\alpha_{eff} = \frac{k_{eff}}{(\rho c_p)_{na}} \tag{16}$$

Additionally, electrical nanofluid conductivity can be obtained from the equation inserted below [74]:

$$\frac{\sigma_{na}}{\sigma_{bf}} = 1 + \frac{3\left(\frac{\sigma_{sp}}{\sigma_{bf}} - 1\right)\phi}{\left(\frac{\sigma_{sp}}{\sigma_{bf}} + 2\right) - \left(\frac{\sigma_{sp}}{\sigma_{bf}} - 1\right)\phi} \tag{17}$$

The thermal boundary conditions that had been applied into the permeable surfaces between the right layer (nanofluid) and the left layer (nanofluid and porous medium) may be defined as inserted below:

$$\theta_{po} = \theta_{na}, \frac{\partial \theta_{na}}{\partial X} = \frac{K_{eff}}{K_{na}} \frac{\partial \theta_{po}}{\partial X}, \Psi_{po} = \Psi_{na}, \frac{\partial \Psi_{na}}{\partial X} = \frac{\partial \Psi_{po}}{\partial X}, \Omega_{po} = \Omega_{na},$$

$$\frac{\partial \Omega_{na}}{\partial X} = \frac{\partial \Omega_{po}}{\partial X}, \mu_{po} \left(\frac{\partial U_{po}}{\partial Y} + \frac{\partial V_{po}}{\partial X} \right) = \mu_{na} \left(\frac{\partial U_{na}}{\partial Y} + \frac{\partial V_{na}}{\partial X} \right), P_{po} = P_{na}, \frac{\partial P_{po}}{\partial X} = \frac{\partial P_{na}}{\partial Y}$$

• **Boundary conditions**

The boundary conditions had been as indicated below:

- The left wall in addition to the inner elliptical body had been kept at isotherm hot temperature
- The right wall had been kept at isotherm cold temperature
- The top and bottom walls are adiabatic

• **Nusselt number**

Nusselt number can be obtained as indicated below along the hot left side wall:

$$Nu_L = \frac{k_{eff}}{k_f} \frac{\partial \theta}{\partial n}, \overline{Nu} = \frac{1}{l} \int_0^l Nu_L(\phi) d\phi \tag{18}$$

Mesh and Validation

The Galerkin finite element formulation used in the present work to solve the dimensionless partial differential equations. Besides, Newton–Raphson method had been utilized to treat the discretized the equations in each layer. The errors of the convergence criteria had been set to be equal to 10⁻⁷ for each variable.

$$\sum \left| \xi_{ij}^{n+1} - \xi_{ij}^n \right| / \left| \xi_{ij}^{n+1} \right| \leq 10^{-7} \tag{19}$$

Numerical grid generation had been presented in Fig. 2a for different four wavy patterns. Also, mesh independent test had been presented in Fig. 2b. The flowchart of the numerical solution is presented in Fig. 2c. The present results based upon CFD code had been validated with significant researchers. Firstly, a validation with the case of inner circular cylinder located within square enclosure in terms of contours (Fig. 3) and Nusselt number (Fig. 4) of the previous results presented by Kim et al. [76]. Secondly, a validation in terms of streamlines of the present CFD code with Nikfar and Mahmoodi [77] had been presented in Fig. 5. Finally, another four validations had been presented in Table 2 in terms of Nusselt number. All of these comparisons reveal

that the present CFD code is in a good agreement with the previous published works.

The average absolute deviation (A.A.D) is an important indicator that reflects the accuracy of the numerical results and it is given by the formula inserted below:

Relative Deviation

$$RD_i = \frac{Nu_{\text{present study}} - Nu_{\text{previous study}}}{Nu_{\text{present study}}} \tag{20}$$

$$\text{Average Absolute Deviation A.A.D.} = \frac{\sum_{i=1}^{i=n} |RD_i|}{n} \tag{21}$$

The maximum absolute deviation (A.A.D.) of this study is 0.007 as indicated in Table 2.

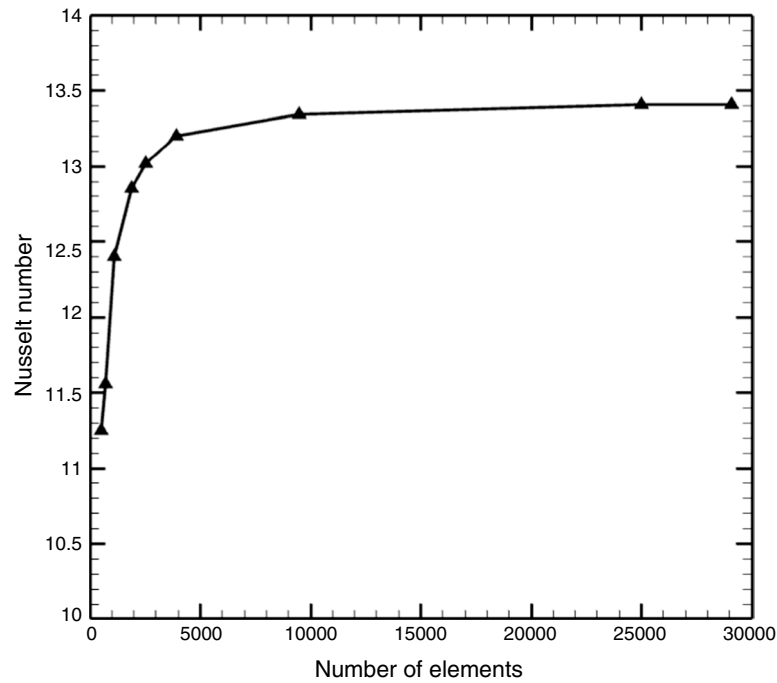
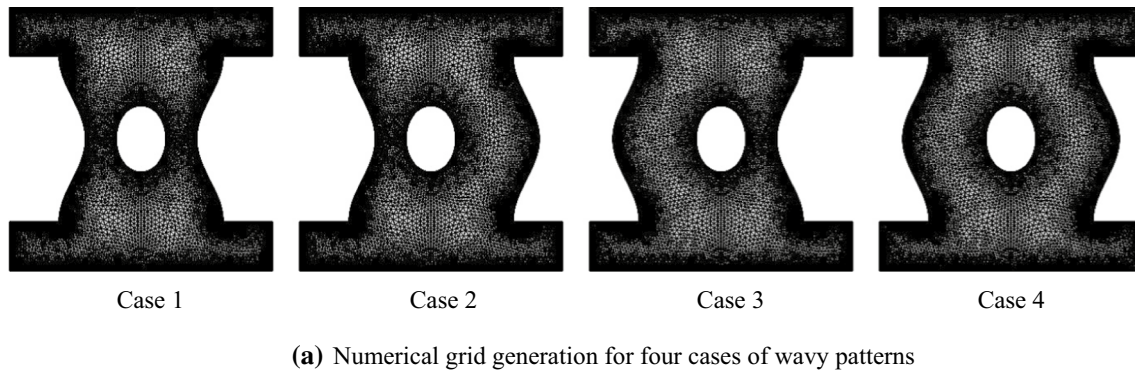


Fig. 2 a Numerical grid generation for four cases of wavy patterns b Mesh independent test for Case 1 c Flowchart of the solution procedure

Results and discussion

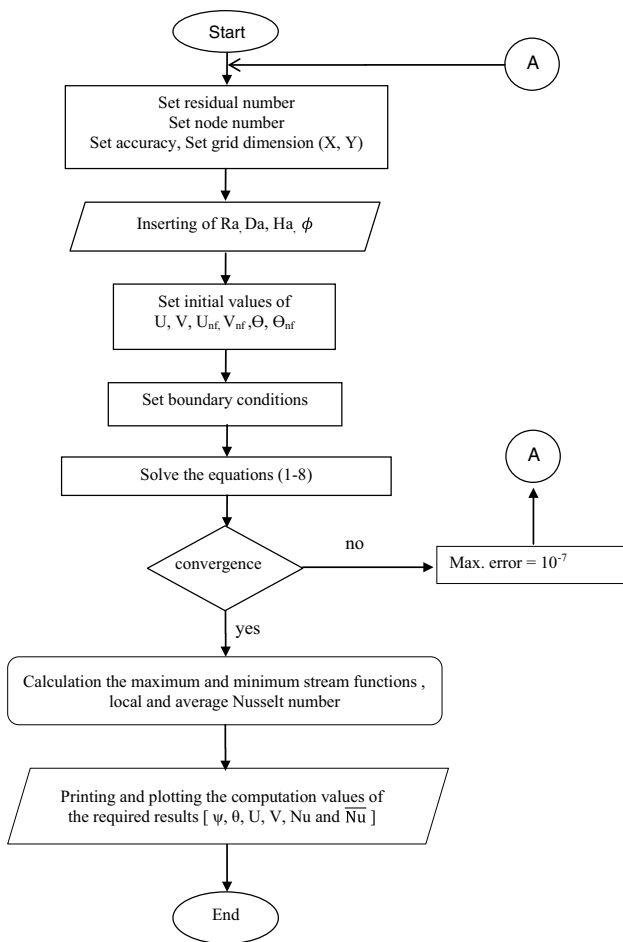
In this section, the influence of various physical in addition to the geometrical dimensionless parameters on fluid flow strength and heat transfer will be discussed in full-details.

The influence of number of undulations

In this section, the influence of number of undulations ($1 \leq N \leq 4$) considering four different cases of wavy patterns on streamlines and isotherms with and without magnetic field had been presented in Figs. 6–9.

Firstly, considering the absence of magnetic field to examine the influence of number of undulations along with the impact of wavy shape patterns on fluid flow strength

and isotherms is presented via Figs. 6 and 7. So regarding the streamlines as shown in Fig. 6, it may be noted that when the number of undulations is ($N = 1$), Case 3 reveals the highest strength in fluid flow as its maximum stream function $|\Psi_{\max}| = 34.229$ while Case 2 reveals the lowest fluid flow strength as its maximum stream function $|\Psi_{\max}| = 30.1766$ which make Case 3 (Out-In) better than Case 2 (In-Out) by 13.42%. The physical reason behind this is due to stenosis between the inner hot elliptical body and the right cold walls which increases the impact between the fluid molecules. It can be seen that increasing the number of undulations beyond ($N = 1$) leads reduce the strength of the fluid flow because increases the wavy surfaces resist the free movement of the nanofluid. Additionally, the influence of wavy patterns is negligible. However, increasing the number



(c) Flow chart of the solution procedure.

Fig. 2 (continued)

of undulations leads to decreasing the fluid flow strength for most of the cases as the area of the wall increases which makes the resistance of internal wavy surfaces increases and resist the movement of nanofluid as its kinetic energy

Fig. 3 A comparison between the present results and Kim et al. [76] in terms of streamlines and isotherms

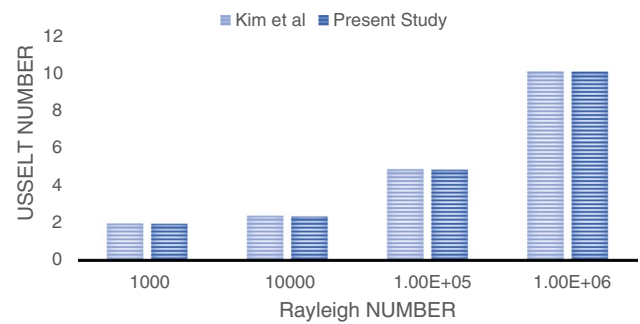
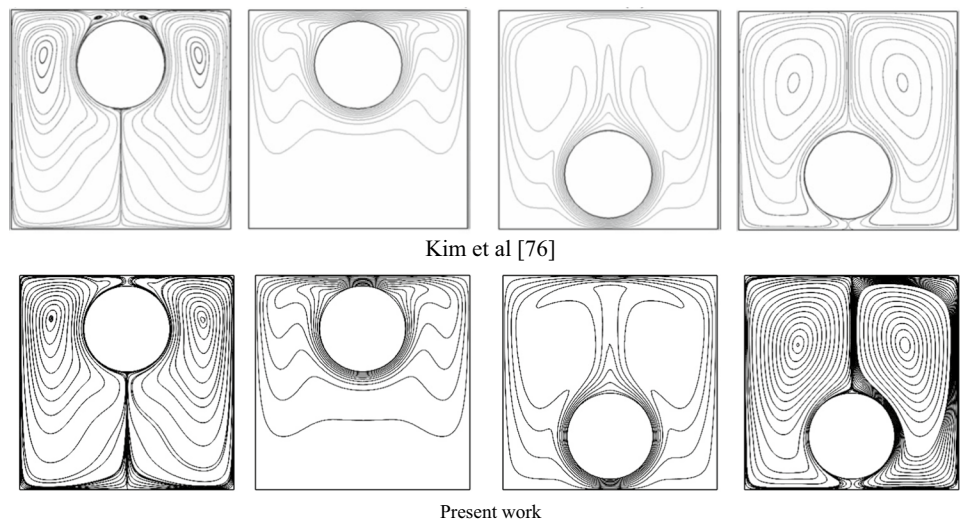


Fig. 4 A comparison between the present results and Kim et al. [76] in terms of Nusselt number

decreases. On the other side, the influences of number of undulations and wavy patterns on isotherms are demonstrated via Fig. 7. It can be seen that the hottest region is on the top area of the enclosure as it denser while the cold isotherms lines are on the lower side of the enclosure. Besides, it can be seen that the wavy patterns completely changes the distribution of isotherms lines in a comparison with the number of undulations.

Secondly, considering the existence of magnetic field to examine the influence of number of undulations along with the impact of wavy shape patterns on fluid flow strength and isotherms is presented via Figs. 8 and 9. It can be seen that the magnetic field at ($Ha = 60$), an obvious reduction for all of the cases of wavy patterns and number of undulations. For example, if a comparison had been made between the stream function with and without magnetic field i.e., at $Ha = 0$ and $Ha = 60$, respectively considering Case 1. It is an obvious the magnetic field reduces the stream function by 48.95%. So, it can be seen that the impact of magnetic field on the fluid flow strength is higher than the impact of wavy patterns and the number of undulations. It can be seen as illustrated in Fig. 9 that the magnetic field changes the distribution of

Fig. 5 Validation of the present results with Nikfar and Mahmoodi [77]

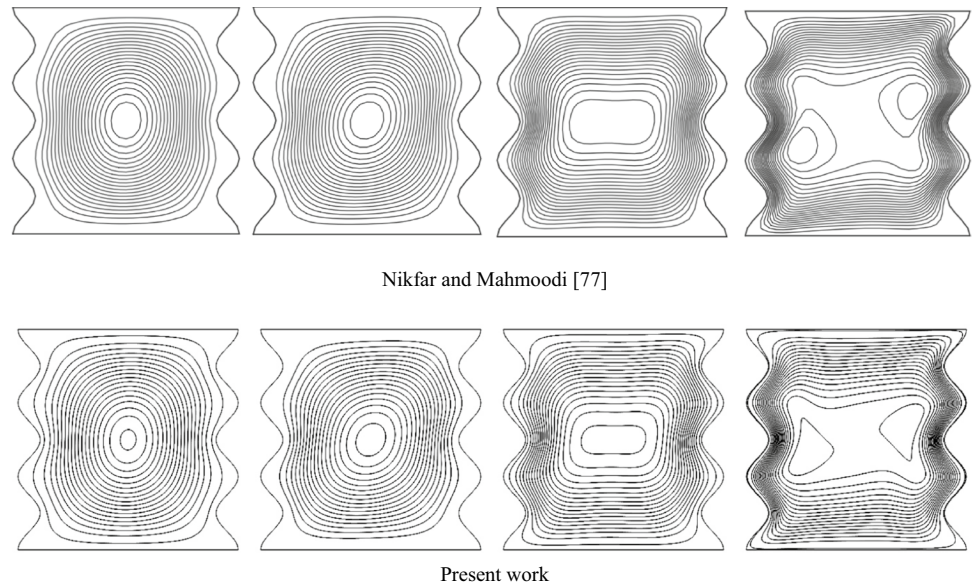


Table 2 Average absolute deviation of the present work with the previous published works

Ra	Nusselt number					A.A.D.%
	Present study	Khanafar [78]	Fusegi [79]	Davis [80]	Barakos [81]	
10^3	1.1178	1.118	1.105	1.118	1.114	0.003802
10^4	2.2449	2.245	2.302	2.243	2.245	0.006592
10^5	4.5221	4.522	4.646	4.519	4.51	0.007695
10^6	8.827	8.826	9.012	8.799	8.806	0.006548

isotherms obviously in a comparison in the case of absence of the magnetic field.

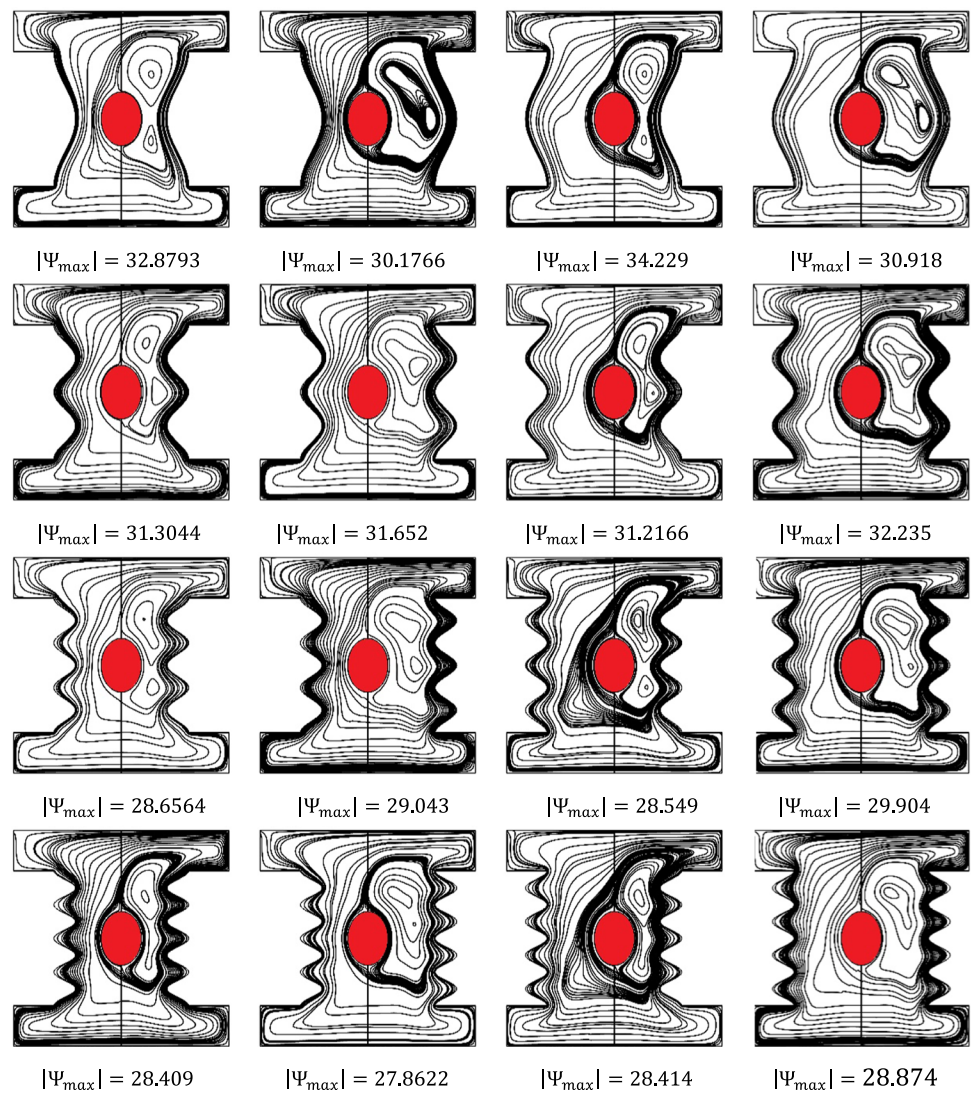
The influence of distance between wavy walls

In this section, the influence of distance between the wavy walls considering four different cases of wavy patterns with and without magnetic field had been presented via Figs. 10, 11, 12 and 13. The number of undulations is fixed to ($N = 1$). The selected distance between wavy walls had been taken as ($B = 0.8 - 1.4$). Considering the absence of magnetic field and regarding Fig. 10, which show the strong relation between the distance between wavy walls and the wavy patterns on the stream function which reveals the strength of the fluid flow. It can be seen that at $B = 0.8$, the stream function values would be for Case 2 > Case 3 > Case 4 > Case 1. Also, regardless the wavy shape patterns, the fluid flow would be at its minimum values when the distance parameter between two wavy walls is at $B = 0.8$. In this way i.e., at $B = 0.8$, Case 1 reveals the lowest fluid flow strength with maximum stream function $|\Psi_{\max}| = 23.270$. This is noted by two inner cells that formed above and below the inner elliptical body because the distance between the elliptical

body and wavy walls too small which break down the natural convection currents into two inner cells. Considering Case 1, it can be seen that increasing the distance parameter between two wavy walls into $B = 1.0$, leads to improve the fluid flow strength by 41.17%. However, further increasing of the wavy walls distance had negligible impact on the fluid flow strength for all cases of wavy patterns. The impact of the distance between the wavy walls on isotherms had been presented in Fig. 11 which clearly influences on their distribution.

The magnetic field taken into account to examine its effect on streamlines and isotherms had been shown via Figs. 12 and 13, respectively. The results when the magnetic field and the distance parameter between the wavy walls are crucial. W.r.t. Figure 12 there are many important point. Firstly, for all four cases of wavy walls, it can be seen that there is increasing in the fluid flow strength with increasing of the distance parameter between wavy walls but in a lower rate in a comparison with the case of the absence of magnetic field that had been illustrated in Fig. 10. For example, taking Case 1 it can be seen that increasing the distance between wavy walls from ($B = 0.8$) into ($B = 1.4$) leads to improve

Fig. 6 Streamlines contours in the absence of magnetic field considering different cases of wavy patterns and different number of undulations at $Ra = 10^6$, $Ha = 0$, $Da = 0.001$, $\phi = 0.02$, $\gamma = 45^\circ$



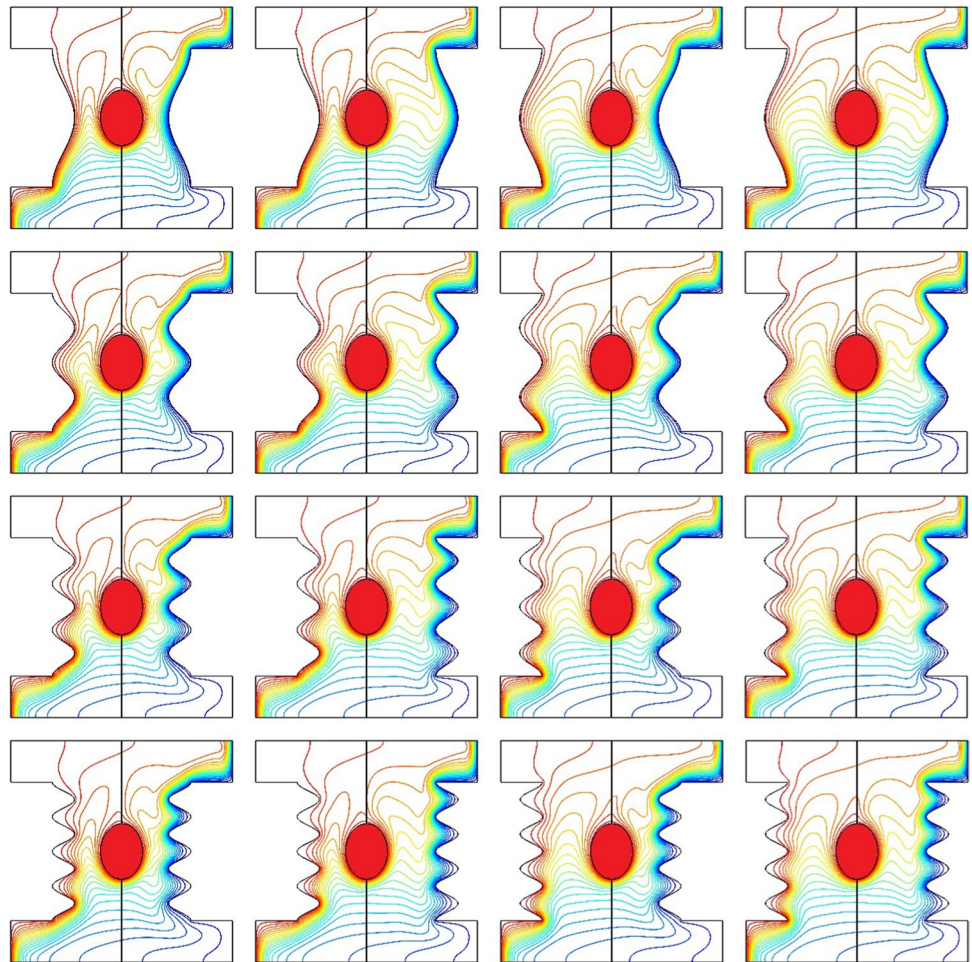
the fluid flow strength by 16.07%. The impact of magnetic field and the distance between wavy walls are presented in Fig. 13 which clearly change the distribution of isotherms in a comparison with the absence of magnetic field.

The influence of inner elliptical body position

The influence of inner elliptical body position on fluid flow and heat transfer had been presented in terms of streamlines and isotherms in Figs. 14 and 15, respectively, for four different cases of wavy walls patterns.

Firstly, w.r.t. Figure 14, it can be seen that for all wavy patterns that moving of the inner elliptical body from the center of the enclosure into the top region leads to an obvious reduction in the fluid flow strength while its movement into the lower region reveals better fluid flow strength. For example, considering Case 1 when the inner body located at the center ($\delta = 0.8$), the absolute maximum stream function $|\Psi_{\max}| = 32.852$ while when it moves into the top at ($\delta = 1.3$), the absolute maximum stream function $|\Psi_{\max}| = 19.304$ while when it moves to the lower

Fig. 7 Isotherms contours in the absence of magnetic field considering different cases of wavy patterns and different number of undulations at $Ra = 10^6$, $Ha = 0$, $Da = 0.001$,

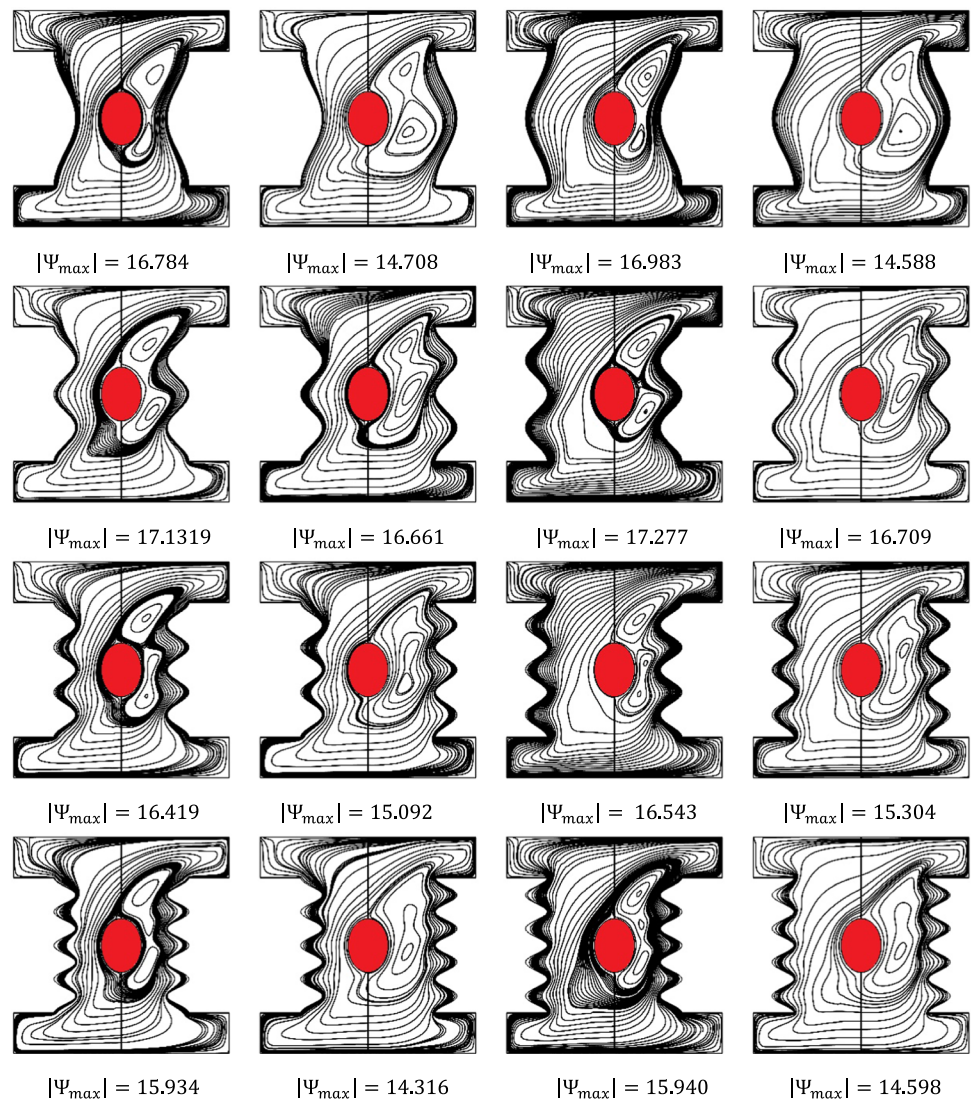


region at ($\delta = 0.3$), the absolute maximum stream function $|\Psi_{\max}| = 34.019$. The same behavior is noted for other wavy patterns. However, the magnitude of fluid flow strength is different from wavy patterns to another patterns along with the position of inner elliptical body. For example, at ($\delta = 0.8$), the fluid flow strength of Case 3 > Case 1 > Case 4 > Case 2 while at ($\delta = 0.3$), Case 4 > Case 2 > Case 3 > Case 1. On the other hand at ($\delta = 1.3$), Case 4 > Case 2 > Case 1 > Case 3. It is also noted that two inner cells had

been created above and below the inner elliptical body when it positioned at the center while these inner cells had been broken into on one inner cell located above the inner body when it moved toward the lower region while the inner cell formed below the inner body when the latter moved toward the top region.

Secondly, w.r.t. isotherms that had been presented in Fig. 15, it can be seen that when the inner body located in the bottom region more hot isotherms lines distributed

Fig. 8 Streamlines contours in the existence of the magnetic field considering different cases of wavy patterns and different number of undulations at $Ra = 10^6$, $Ha = 60$, $Da = 0.001$, $\gamma = 45^\circ$, $\phi = 0.02$



among the area of the enclosure while location of the inner body in the top region leads to a lot of cold isotherms lines fill the enclosure area.

The influence of selected parameters on Nusselt number

The most important dimensionless parameter in heat transfer analysis which in the indicator of heat transfer bettering is Nusselt number. So, this section will explain this idea in full details.

The influence of different wavy patterns along with the number of undulations in the absence of magnetic field i.e., at ($Ha = 0$) had been shown in Fig. 16. It can be seen that

increasing the number of undulations reduces the Nusselt number which turn in reduction of heat transfer. It can be seen that when the number of undulations is ($N = 1$), the Nusselt number of Case 3 > Case 1 > Case 4 > Case 2. This behavior of Nusselt number remains the same when the number of undulations increases into ($N = 2$). However, increasing the number of undulations into ($N = 3$), make Nusselt number of wavy shape of Case 1 had the highest value in a comparison with that of Case 2 which had the lowest Nusselt number. While increasing the number of undulations into ($N = 4$) leads to make Nusselt number of Case 3 had the highest value along with keeping Case 2 had the lowest Nusselt number. It can see that based upon the numerical observations that in the absence of magnetic field

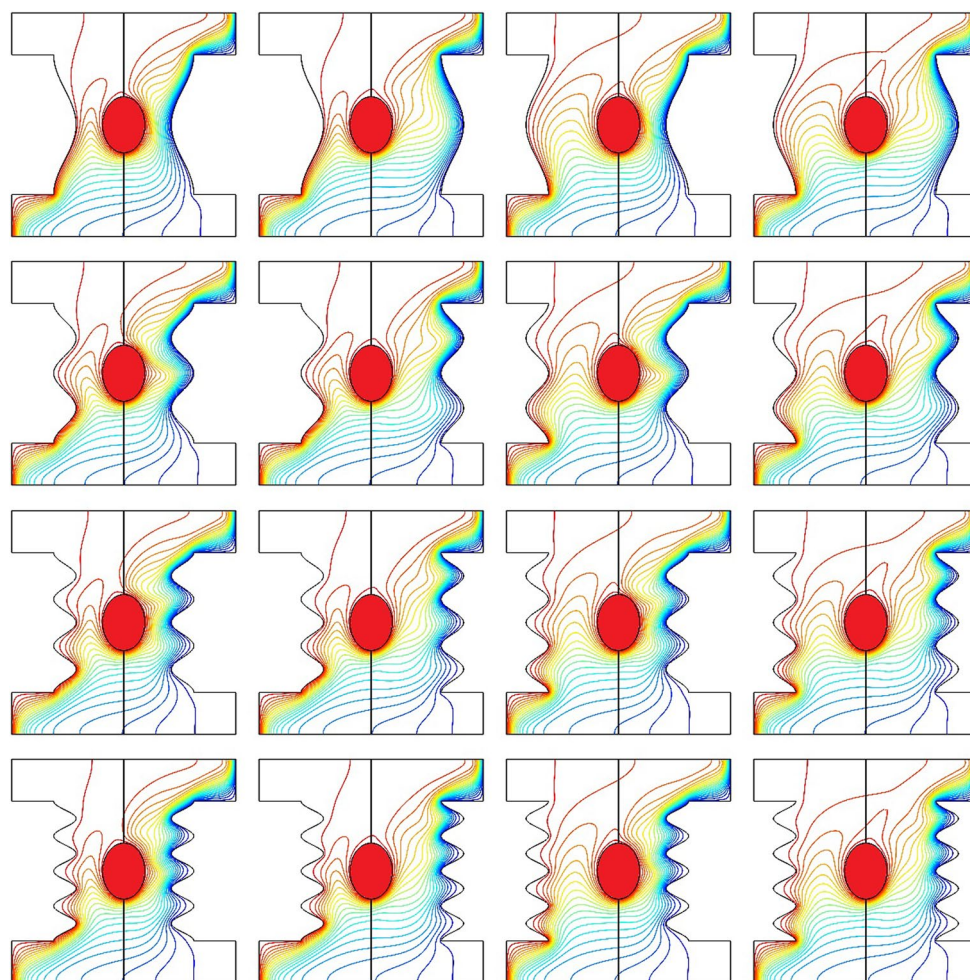


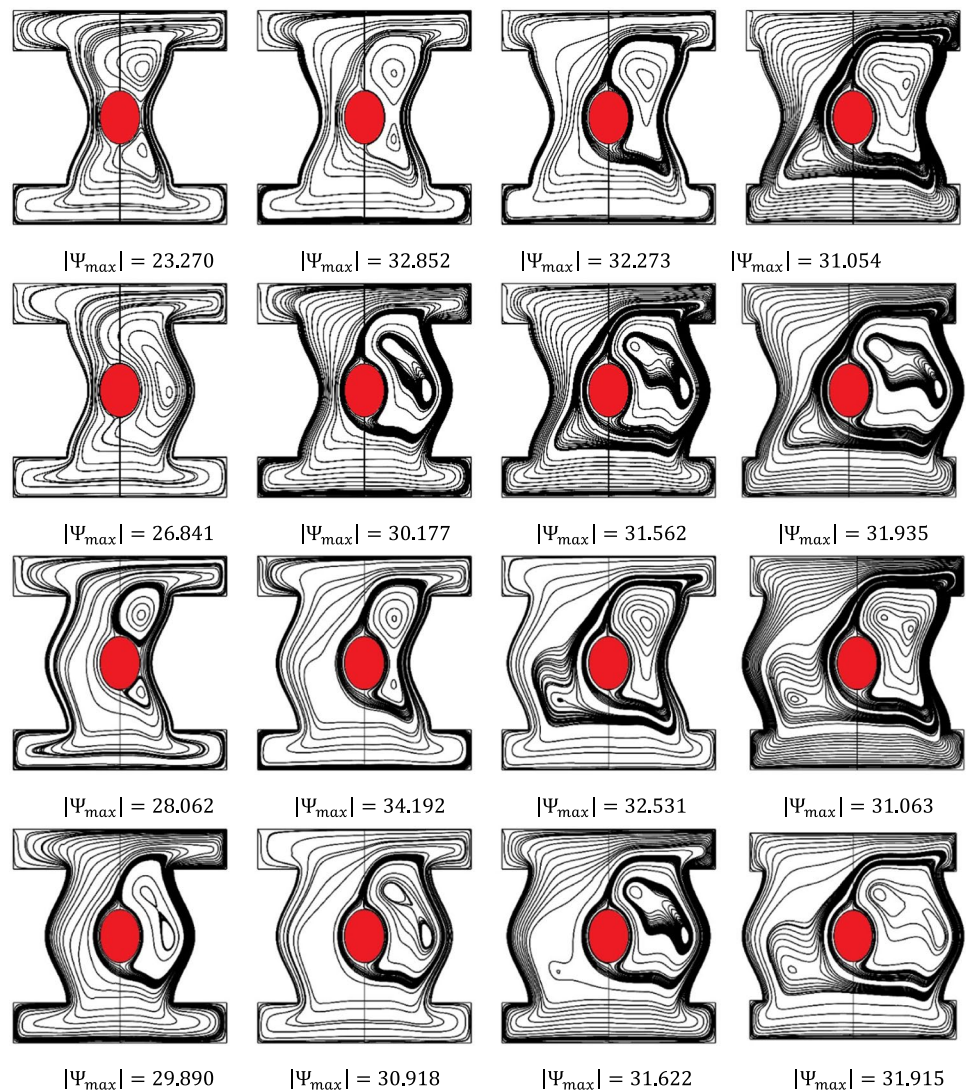
Fig. 9 Isotherm lines contours in the existence of the magnetic field considering different cases of wavy patterns and different number of undulations at $Ra = 10^6$, $Ha = 60$, $Da = 0.001$, $\gamma = 45^\circ$, $\phi = 0.02$

that the influence of number of undulations and the wavy patterns are high as illustrated in Fig. 16. While considering the influence of magnetic field at Fig. 17 which reveals that the impact of magnetic field is higher than the influence of wavy walls patterns. For example, when the number of undulations are ($N = 3, 4$), there are similar contribution on Nusselt number for Case 1 and Case 2. As well as approximately similar value of Nusselt number for Case 3 and Case

4. Additionally, Nusselt number of Case 3 and Case 4 are higher than that of Case 1 and Case 2.

The influence of the distance between the wavy walls had been shown via Figs. 18 and 19 without and with magnetic field, respectively. Considering Fig. 18, it can be seen that increasing the distance between wavy walls for all four cases of the wavy patterns leads to enhance the heat transfer by increasing the dimensionless value of

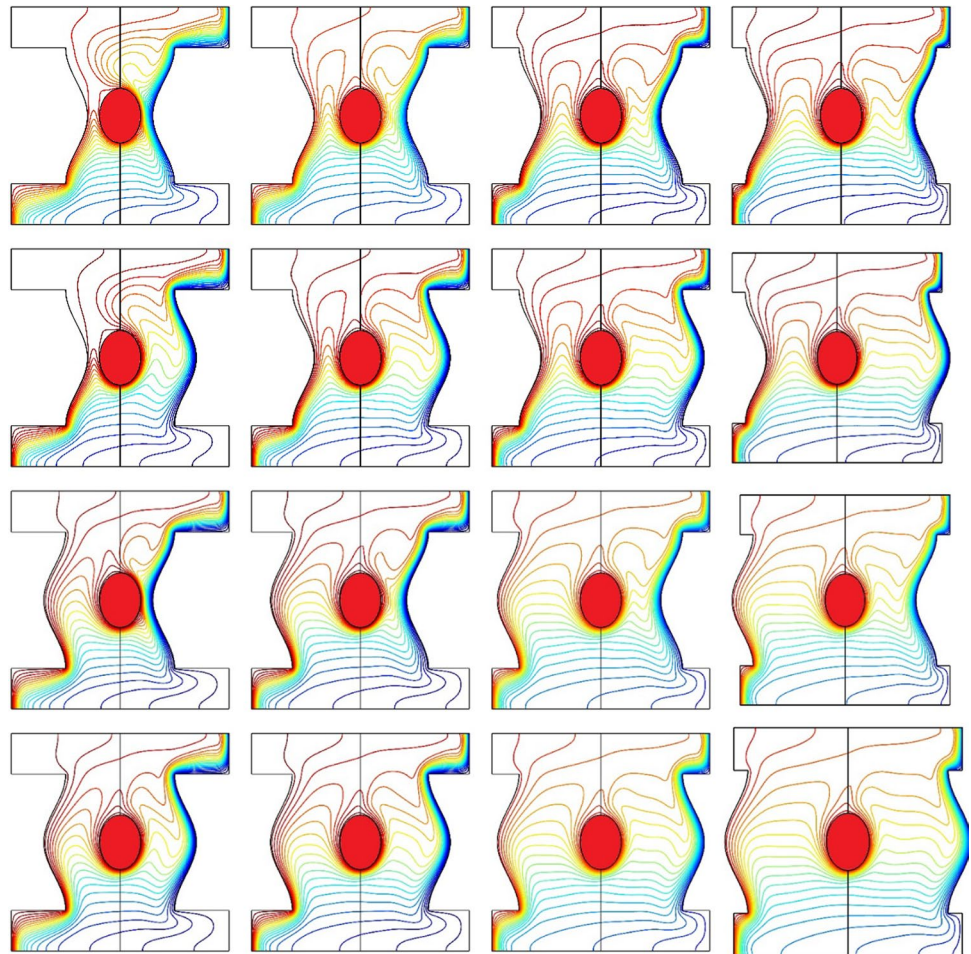
Fig. 10 Streamlines contours in the absence of the magnetic field considering different cases of wavy patterns and different distance between wavy patterns at $Ra = 10^6$, $Ha = 0$, $Da = 0.001$, $\gamma = 45^\circ$, $\phi = 0.02$



Nusselt number. For example, for Case 1 increasing the distance from $B = 0.8$ into $B = 1.4$ leads to increase Nusselt number by 31.67%. On the other hands when the magnetic field effect taken into account as shown in Fig. 19, it can be seen that still increasing the distance between the wavy patterns enhance Nusselt number but lower than that in the absence of magnetic field. It is worthy to mention that in the existence of the magnetic field, Case 4 had the lowest Nusselt number in a comparison with the other cases of wavy patterns.

The impact of the position of inner body is illustrated via Figs. 20 and 21 without and with the magnetic field, respectively. Three different positions of inner elliptical body had been selected which they are at the center ($\delta = 0.8$), at the top region ($\delta = 1.3$), at the bottom region ($\delta = 0.3$). It can be seen for Case 1 as shown in Fig. 20 that when the inner elliptical body moves from the center into the top, Nusselt number decreases from $Nu = 14.8685$ into $Nu = 7.5926$ while movement the inner elliptical body from the center top into

Fig. 11 Isotherm lines contours in the absence of the magnetic field considering different cases of wavy patterns and different distance between wavy patterns at $Ra = 10^6$, $Ha = 0$, $Da = 0.001$, $\gamma = 45^\circ$, $\phi = 0.02$



the bottom leads to enhance the heat transfer rate by increasing of Nusselt number about 67.70%. In this way, it can be seen that the similar trends is observed for all wavy patterns. Also, in Fig. 21 which show the behavior of Nusselt number with the position of inner elliptical body inner the influence

of magnetic field. It may be noted that the magnetic field make a notice difference and the influence of wavy shape patterns more strong in a comparison of that in the absence of magnetic field.

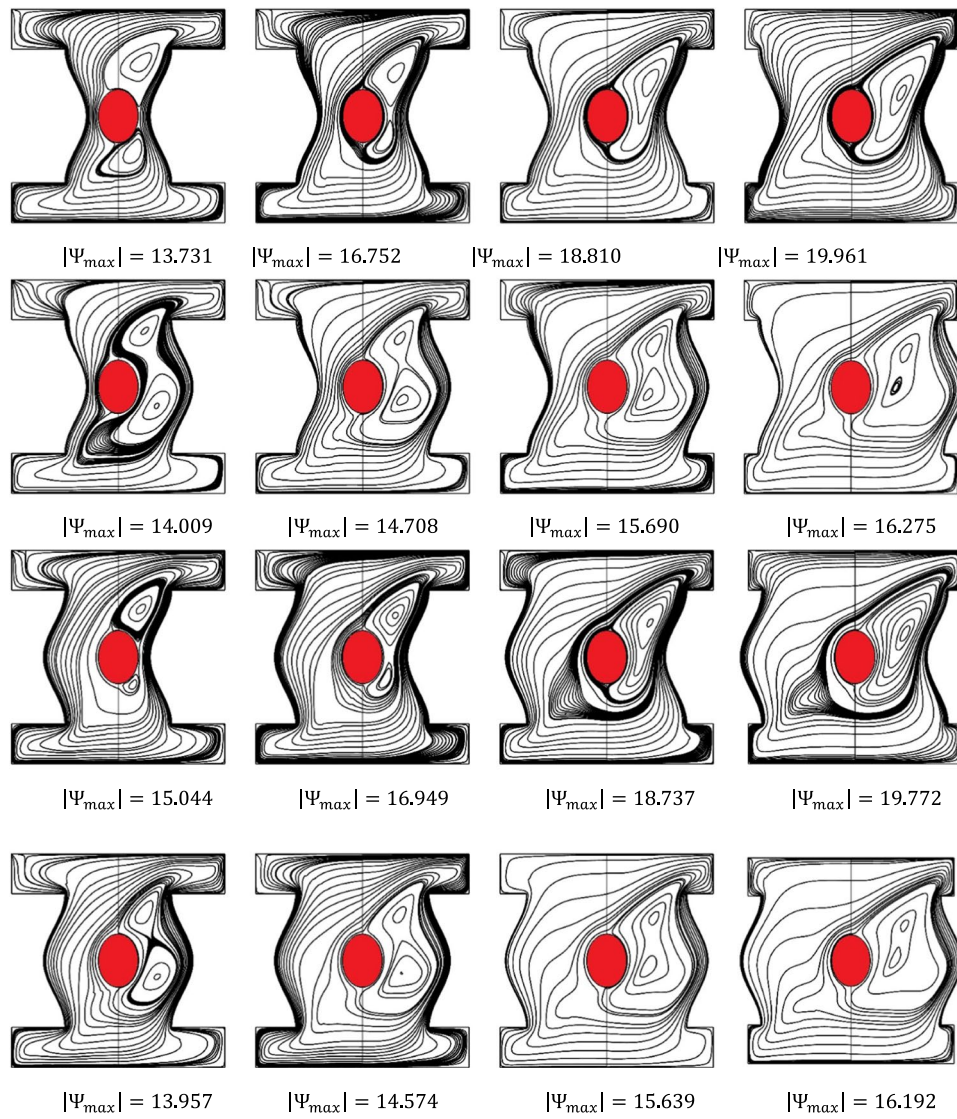
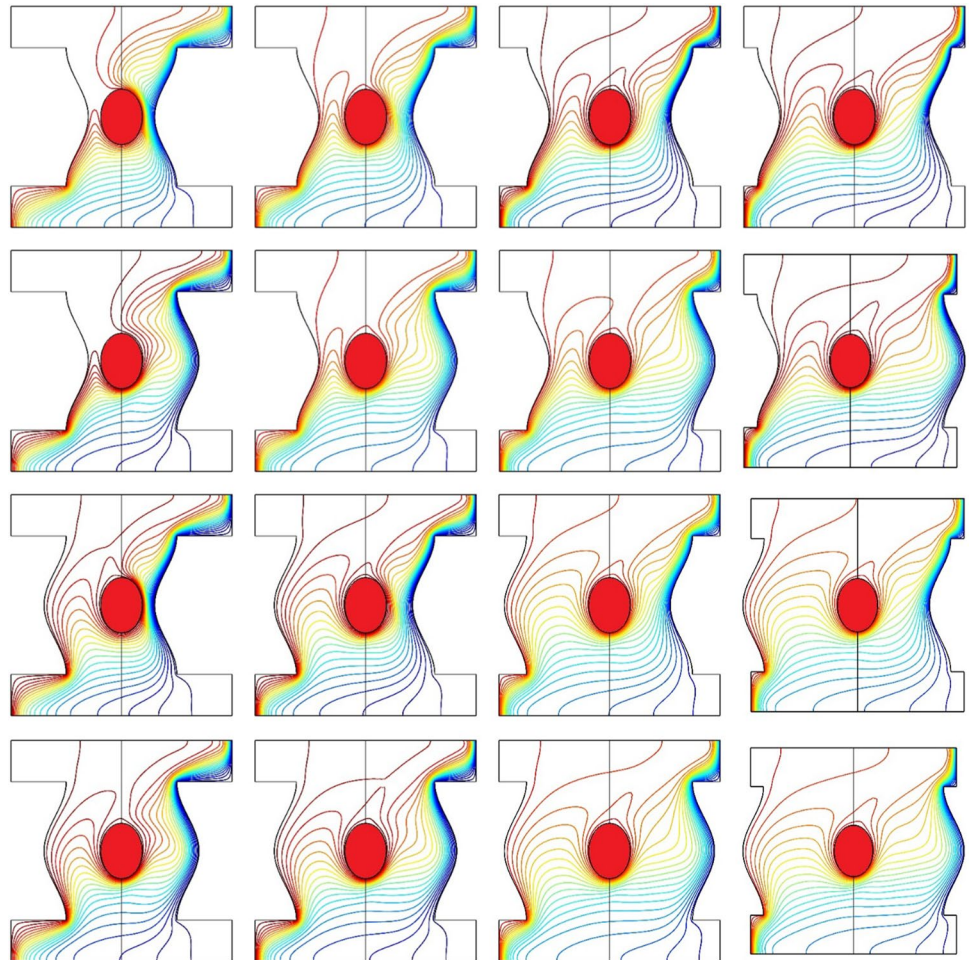


Fig. 12 Streamlines contours in the existence of the magnetic field considering different cases of wavy patterns and different distance between wavy patterns at $Ra = 10^6$, $Ha = 60$, $Da = 0.001$, $\gamma = 45^\circ$, $\phi = 0.02$

Fig. 13 Isotherm lines contours in the existence of the magnetic field considering different cases of wavy patterns and different distance between wavy patterns at $Ra = 10^6$, $Ha = 60$, $Da = 0.001$, $\gamma = 45^\circ$, $\phi = 0.02$



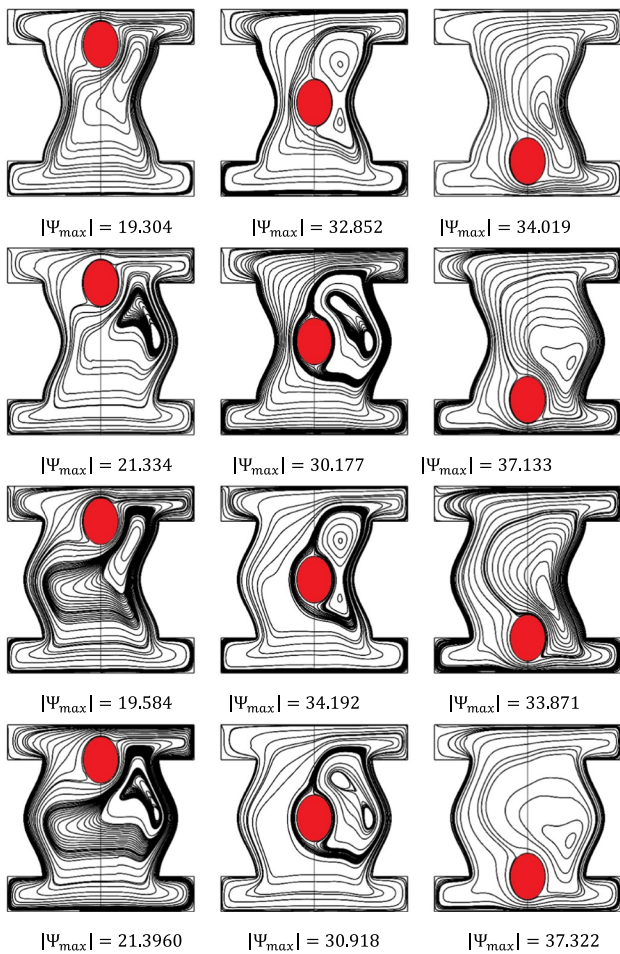


Fig. 14 Streamlines contours considering different cases of wavy patterns under different position of inner elliptical body at $Ra = 10^6, Ha = 0, Da = 0.001, \gamma = 45^\circ, \phi = 0.02$

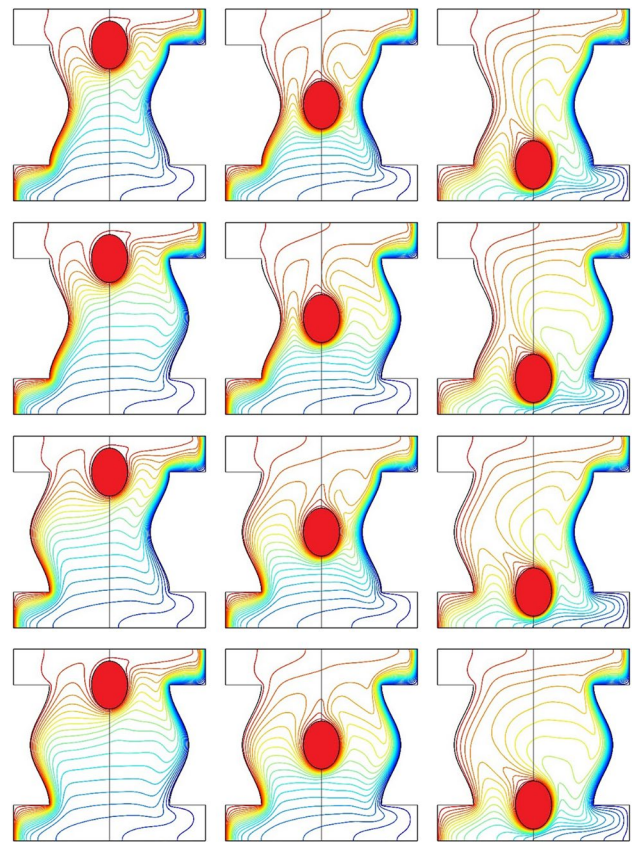


Fig. 15 Isotherm lines contours considering different cases of wavy patterns under different position of inner elliptical body at $Ra = 10^6, Ha = 0, Da = 0.001, \gamma = 45^\circ, \phi = 0.02$

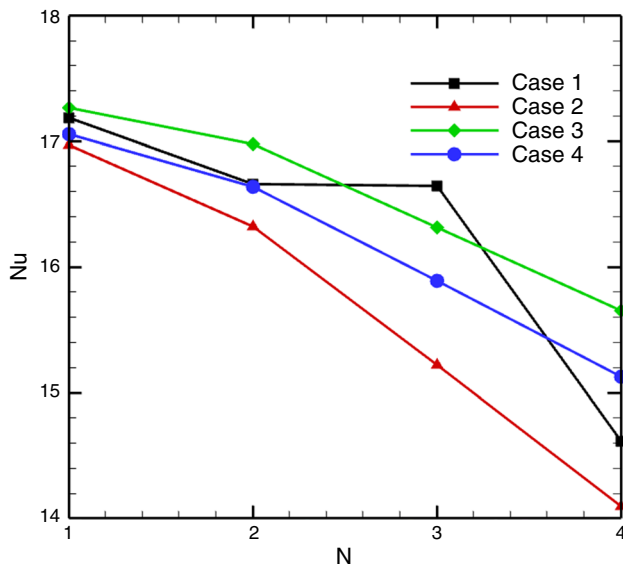


Fig. 16 Nusselt number variation w.r.t. number of undulations considering different cases of wavy patterns in the absence of magnetic field at $Ra = 10^6, Da = 0.001, Ha = 0, \gamma = 45^\circ$

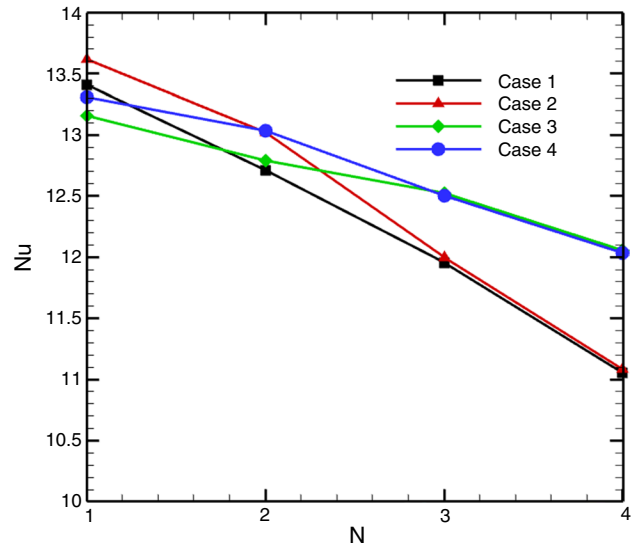


Fig. 17 Nusselt number variation w.r.t. number of undulations considering different cases of wavy patterns in the existence of magnetic field at $Ra = 10^6, Da = 0.001, Ha = 60, \gamma = 45^\circ$

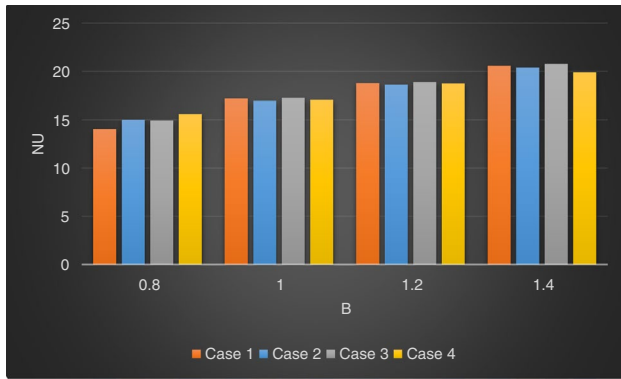


Fig. 18 Nusselt number variation w.r.t. distance between wavy walls considering different cases of wavy patterns in the absence of magnetic field at $Ra = 10^6$, $Da = 0.001$, $Ha = 0$

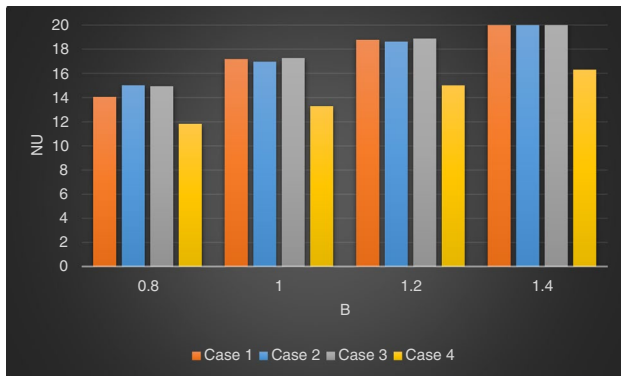


Fig. 19 Nusselt number variation w.r.t. distance between wavy walls considering different cases of wavy patterns in the existence of magnetic field at $Ra = 10^6$, $Da = 0.001$, $Ha = 60$, $\gamma = 45^\circ$

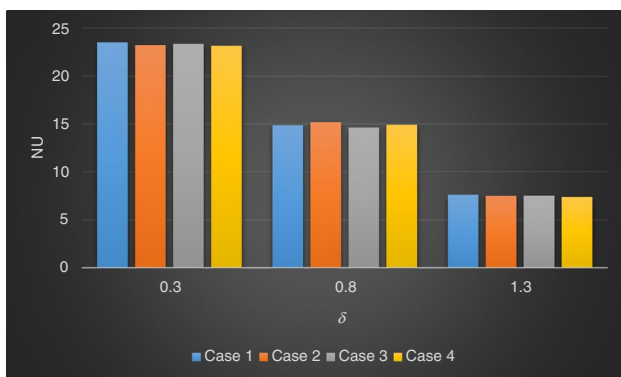


Fig. 20 Nusselt number variation w.r.t. vertical position of the elliptical inner body considering different cases of wavy patterns in the absence of magnetic field at $Ra = 10^6$, $Da = 0.001$, $Ha = 0$

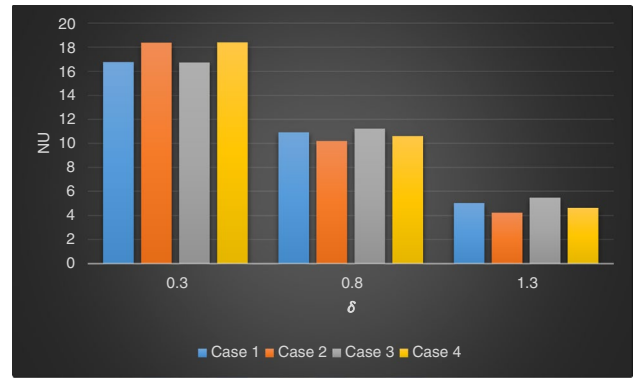


Fig. 21 Nusselt number variation w.r.t. vertical position of the elliptical inner body considering different cases of wavy patterns in the existence of magnetic field at $Ra = 10^6$, $Da = 0.001$, $Ha = 60$, $\gamma = 45^\circ$

Conclusions

The present work examines numerically the influence of wavy patterns on fluid flows and heat transfer considering the existence of inner elliptical body under the impact of magnetic field. The major results can be summarized as indicated below:

- The influence of wavy shape patterns is higher when the number of undulations ($N = 1$).
- Case 3 is highest than Case 2 by 13.42% in terms of fluid flow strength.
- Increasing Hartmann number from $Ha = 0$ into $Ha = 60$ leads to an obvious reduction in the fluid flow by 48.95%.
- Case 4 along with locating the inner elliptical body in the bottom of the enclosure reveals the best strength in the fluid flow.
- For bettering the thermal rate of heat transfer, it is recommended to move the inner elliptical body downwards for all cases of wavy patterns.
- Increasing the number of undulations along with Hartmann number reduces the heat transfer rate.
- Nusselt number improved with increasing the parameter of the distance between the wavy walls

Acknowledgements The authors thank University of Babylon for giving them the opportunity, time and scientific support for completing this work and Al-Mustaqbal University College for their support.

Funding The authors extend their appreciation to the Deanship of Scientific Research at King Khalid University, Saudi Arabia for funding this work through Large Groups (Project under grant number RGP.2/24/1443).

References

- Basak T, Ayappa KG. Influence of internal convection during microwave thawing of cylinders. *AIChE J.* 2001;47(4):835–50.
- Pirathepan M, Anderson TN. Natural convection heat transfer in façade integrated solar concentrators. *Sol Energy.* 2015;122:271–6. <https://doi.org/10.1016/j.solener.2015.09.008>.
- Al-Kayiem HH, Yassen TA. On the natural convection heat transfer in a rectangular passage solar air heater. *Sol Energy.* 2015;112:310–8. <https://doi.org/10.1016/j.solener.2014.11.031>.
- Budihardjo I, Morrison GL, Behnia M. Natural circulation flow through water-in-glass evacuated tube solar collectors. *Sol Energy.* 2007;81(12):1460–72. <https://doi.org/10.1016/j.solener.2007.03.002>.
- Tao YB, He YL. Numerical study on coupled fluid flow and heat transfer process in parabolic trough solar collector tube. *Sol Energy.* 2010;84(10):1863–72. <https://doi.org/10.1016/j.solener.2010.07.012>.
- Al-Ansary H, Zeitoun O. Numerical study of conduction and convection heat losses from a half-insulated air-filled annulus of the receiver of a parabolic trough collector. *Sol Energy.* 2011;85(11):3036–45. <https://doi.org/10.1016/j.solener.2011.09.002>.
- Horta P, Henriques JCC, Collares-Pereira M. Impact of different internal convection control strategies in a non-evacuated CPC collector performance. *Sol Energy.* 2012;86(5):1232–44. <https://doi.org/10.1016/j.solener.2012.01.016>.
- Li B, Oliveira FAC, Rodríguez J, Fernandes JC, Rosa LG. Numerical and experimental study on improving temperature uniformity of solar furnaces for materials processing. *Sol Energy.* 2015;115:95–108. <https://doi.org/10.1016/j.solener.2015.02.023>.
- Joneidi AA, Domairry G, Babelahi M. Analytical treatment of MHD free convective flow and mass transfer over a stretching sheet with chemical reaction. *J Taiwan Inst Chem Eng.* 2010;41(1):35–43. <https://doi.org/10.1016/j.jtice.2009.05.008>.
- Nadeem S, Saleem S. Analytical treatment of unsteady mixed convection MHD flow on a rotating cone in a rotating frame. *J Taiwan Inst Chem Eng.* 2013;44(4):596–604. <https://doi.org/10.1016/j.jtice.2013.01.007>.
- Sarafraz MM, Christo F. Thermal and flow characteristics of liquid flow in a 3D-printed micro-reactor: a numerical and experimental study. *Appl Therm Eng.* 2021;199: 117531.
- Sarafraz MM, Hormozi F, Peyghambarzadeh SM. Pool boiling heat transfer to aqueous alumina nano-fluids on the plain and concentric circular micro-structured (CCM) surfaces. *Exp Thermal Fluid Sci.* 2016;72:125–39. <https://doi.org/10.1016/j.expthermflusc.2015.11.001>.
- Mehrzi AA, Farhadi M, Sedighi K, Delavar MA. Effect of fin position and porosity on heat transfer improvement in a plate porous media heat exchanger. *J Taiwan Inst Chem Eng.* 2013;44(3):420–31. <https://doi.org/10.1016/j.jtice.2012.12.018>.
- Abdesslem J, Khalifa S, Abdelaziz N, Abdallah M. Radiative properties effects on unsteady natural convection inside a saturated porous medium Application for porous heat exchangers. *Energy.* 2013;61:224–33. <https://doi.org/10.1016/j.energy.2013.09.015>.
- Dastmalchi M, Sheikhzadeh GA, Abbasian Arani AA. Double-diffusive natural convective in a porous square enclosure filled with nanofluid. *Int J Therm Sci.* 2015;95:88–98. <https://doi.org/10.1016/j.ijthermalsci.2015.04.002>.
- Fontes DH, dos Santos DDO, Martínez Padilla EL, Bandarra Filho EP. Two numerical modelings of free convection heat transfer using nanofluids inside a square enclosure. *Mech Res Commun.* 2015;66:34–43. <https://doi.org/10.1016/j.mechrescom.2015.03.009>.
- Nazari S, Ellahi R, Sarafraz M, Safaei MR, Asgari A, Akbari OA. Numerical study on mixed convection of a non-Newtonian nanofluid with porous media in a two lid-driven square cavity. *J Therm Anal Calorim.* 2020;140(3):1121–45.
- MA Teamah. Numerical simulation of double diffusive natural convection in rectangular enclosure in the presences of magnetic field and heat source. *Int J Therm Sci.* 2008;47(3):237–48. <https://doi.org/10.1016/j.ijthermalsci.2007.02.003>.
- Alam P, Kumar A, Kapoor S, Ansari SR. Numerical investigation of natural convection in a rectangular enclosure due to partial heating and cooling at vertical walls. *Commun Nonlinear Sci Numer Simul.* 2012;17(6):2403–14. <https://doi.org/10.1016/j.cnsns.2011.09.004>.
- Salari M, Malekshah EH, Malekshah MH. Natural convection in a rectangular enclosure filled by two immiscible fluids of air and Al₂O₃-water nanofluid heated partially from side walls. *Alex Eng J.* 2018;57(3):1401–12. <https://doi.org/10.1016/j.aej.2017.07.004>.
- Basak T, Anandalakshmi R, Roy M. Heatlines based natural convection analysis in tilted isosceles triangular enclosures with linearly heated inclined walls: effect of various orientations. *Int Commun Heat Mass Transfer.* 2013;43:39–45. <https://doi.org/10.1016/j.icheatmasstransfer.2013.01.008>.
- Basak T, Roy S, Matta A, Pop I. Analysis of heatlines for natural convection within porous trapezoidal enclosures: effect of uniform and non-uniform heating of bottom wall. *Int J Heat Mass Transf.* 2010;53(25–26):5947–61.
- Natarajan SK, Reddy KS, Mallick TK. Heat loss characteristics of trapezoidal cavity receiver for solar linear concentrating system. *Appl Energy.* 2012;93:523–31. <https://doi.org/10.1016/j.apenergy.2011.12.011>.
- Mejbel AI, Abdulkadhim A, Hamzah RA, Hamzah HK, Ali FH. Natural convection heat transfer for adiabatic circular cylinder inside trapezoidal enclosure filled with nanofluid superposed porous-nanofluid layer. *FME Transactions.* 2020;48(1):82–9.
- Anandalakshmi R, Basak T. Analysis of energy management via entropy generation approach during natural convection in porous rhombic enclosures. *Chem Eng Sci.* 2012;79:75–93. <https://doi.org/10.1016/j.ces.2012.04.029>.
- Ghasemi E, Soleimani S, Baramia H. Natural convection between a circular enclosure and an elliptic cylinder using Control Volume based Finite Element Method. *Int Commun Heat Mass Transfer.* 2012;39(8):1035–44. <https://doi.org/10.1016/j.icheatmasstransfer.2012.06.016>.
- Gupta N, Nayak AK. Activity of buoyancy convection and entropy generation in a parallelogrammic shaped mixed displacement ventilated system. *Int J Therm Sci.* 2019;137:86–100. <https://doi.org/10.1016/j.ijthermalsci.2018.11.006>.
- Sheikholeslami M, Ellahi R, Hassan M, Soleimani S. A study of natural convection heat transfer in a nanofluid filled enclosure with elliptic inner cylinder. *Int J Num Method Heat Fluid Flow.* 2014;24(8):1906–27.
- Rozati SA, Montazerifar F, Ali Akbari O, Hoseinzadeh S, Nikkhal V, Marzban A et al. Natural convection heat transfer of water/Ag nanofluid inside an elliptical enclosure with different attack angles. *Math Method Appl Sci.* 2020.
- Sadeghi MS, Tayebi T, Dogonchi AS, Armaghani T, Talebizadehsardari P. Analysis of hydrothermal characteristics of magnetic Al₂O₃-H₂O nanofluid within a novel wavy enclosure during natural convection process considering internal heat generation. *Math Method Appl Sci.* 2020.
- Goodarzi M, Safaei M, Oztop HF, Karimipour A, Sadeghinezhad E, Dahari M et al. Numerical study of entropy generation due to coupled laminar and turbulent mixed convection and thermal radiation in an enclosure filled with a semitransparent medium. *Sci World J.* 2014

32. Goodarzi M, Safaei M, Karimipour A, Hooman K, Dahari M, Kazi S et al., editors. Comparison of the finite volume and lattice Boltzmann methods for solving natural convection heat transfer problems inside cavities and enclosures. *Abstract Applied Analysis*; 2014: Hindawi
33. Pordanjani AH, Vahedi SM, Rikhtegar F, Wongwises S. Optimization and sensitivity analysis of magneto-hydrodynamic natural convection nanofluid flow inside a square enclosure using response surface methodology. *J Therm Anal Calorim*. 2019;135(2):1031–45.
34. Goodarzi H, Akbari OA, Sarafraz MM, Karchegani MM, Safaei MR, Sheikh Shabani GA. Numerical simulation of natural convection heat transfer of nanofluid with Cu, MWCNT, and Al₂O₃ nanoparticles in a cavity with different aspect ratios. *J Therm Sci Eng Appl*. 2019;11(6):061020.
35. Mehryan S, Ghalambaz M, Izadi M. Conjugate natural convection of nanofluids inside an enclosure filled by three layers of solid, porous medium and free nanofluid using Buongiorno's and local thermal non-equilibrium models. *J Therm Anal Calorim*. 2019;135(2):1047–67.
36. Hussain SH, Rahomey MS. Comparison of natural convection around a circular cylinder with different geometries of cylinders inside a square enclosure filled with Ag-nanofluid superposed porous-nanofluid layers. *J Heat Transfer*. 2019;141(2):022501.
37. Oztop HF, Abu-Nada E, Varol Y, Chamkha A. Natural convection in wavy enclosures with volumetric heat sources. *Int J Therm Sci*. 2011;50(4):502–14.
38. Esmailpour M, Abdollahzadeh M. Free convection and entropy generation of nanofluid inside an enclosure with different patterns of vertical wavy walls. *Int J Therm Sci*. 2012;52:127–36.
39. Kashani S, Ranjbar A, Mastiani M, Mirzaei H. Entropy generation and natural convection of nanoparticle-water mixture (nanofluid) near water density inversion in an enclosure with various patterns of vertical wavy walls. *Appl Math Comput*. 2014;226:180–93.
40. Cho C-C, Chen C-L. Natural convection heat transfer and entropy generation in wavy-wall enclosure containing water-based nanofluid. *Int J Heat Mass Transf*. 2013;61:749–58.
41. Bhardwaj S, Dalal A, Pati S. Influence of wavy wall and non-uniform heating on natural convection heat transfer and entropy generation inside porous complex enclosure. *Energy*. 2015;79:467–81.
42. Sheremet MA, Oztop H, Pop I. MHD natural convection in an inclined wavy cavity with corner heater filled with a nanofluid. *J Magn Magn Mater*. 2016;416:37–47.
43. Sheikholeslami M, Oztop HF. MHD free convection of nanofluid in a cavity with sinusoidal walls by using CVFEM. *Chin J Phys*. 2017;55(6):2291–304. <https://doi.org/10.1016/j.cjph.2017.09.006>.
44. Sheremet M, Cimpean D, Pop I. Free convection in a partially heated wavy porous cavity filled with a nanofluid under the effects of Brownian diffusion and thermophoresis. *Appl Therm Eng*. 2017;113:413–8.
45. Alrowaili D, Ahmed SE, Elshehabey HM, Ezzeldien M. Magnetic radiative buoyancy-driven convection of MWCNTs -C₂H₆O₂ power-law nanofluids in inclined enclosures with wavy walls. *Alex Eng J*. 2022;61(11):8677–89. <https://doi.org/10.1016/j.aej.2022.01.073>.
46. Hatami M. Nanoparticles migration around the heated cylinder during the RSM optimization of a wavy-wall enclosure. *Adv Powder Technol*. 2017;28(3):890–9. <https://doi.org/10.1016/j.apt.2016.12.015>.
47. Alsabery AI, Tayebi T, Chamkha AJ, Hashim I. Effect of rotating solid cylinder on entropy generation and convective heat transfer in a wavy porous cavity heated from below. *Int Commun Heat Mass Transfer*. 2018;95:197–209. <https://doi.org/10.1016/j.icheatmasstransfer.2018.05.003>.
48. Abdulkadhim A, Hamzah HK, Ali FH, Yıldız Ç, Abed AM, Abed EM, et al. Effect of heat generation and heat absorption on natural convection of Cu-water nanofluid in a wavy enclosure under magnetic field. *Int Commun Heat Mass Transfer*. 2021;120: 105024. <https://doi.org/10.1016/j.icheatmasstransfer.2020.105024>.
49. Mokaddes Ali M, Akhter R, Alim MA. Hydromagnetic natural convection in a wavy-walled enclosure equipped with hybrid nanofluid and heat generating cylinder. *Alex Eng J*. 2021;60(6):5245–64. <https://doi.org/10.1016/j.aej.2021.04.059>.
50. Roy NC. Natural convection in the annulus bounded by two wavy wall cylinders having a chemically reacting fluid. *Int J Heat Mass Transf*. 2019;138:1082–95. <https://doi.org/10.1016/j.ijheatmasstransfer.2019.04.133>.
51. Abdulkadhim A, Hamzah HK, Ali FH, Abed AM, Abed IM. Natural convection among inner corrugated cylinders inside wavy enclosure filled with nanofluid superposed in porous-nanofluid layers. *Int Commun Heat Mass Transfer*. 2019;109: 104350. <https://doi.org/10.1016/j.icheatmasstransfer.2019.104350>.
52. Alsabery AI, Mohebbi R, Chamkha AJ, Hashim I. Effect of local thermal non-equilibrium model on natural convection in a nanofluid-filled wavy-walled porous cavity containing inner solid cylinder. *Chem Eng Sci*. 2019;201:247–63. <https://doi.org/10.1016/j.ces.2019.03.006>.
53. Dogonchi AS. Heat transfer by natural convection of Fe₃O₄-water nanofluid in an annulus between a wavy circular cylinder and a rhombus. *Int J Heat Mass Transf*. 2019;130:320–32. <https://doi.org/10.1016/j.ijheatmasstransfer.2018.10.086>.
54. Hashim I, Alsabery AI, Sheremet MA, Chamkha AJ. Numerical investigation of natural convection of Al₂O₃-water nanofluid in a wavy cavity with conductive inner block using Buongiorno's two-phase model. *Adv Powder Technol*. 2019;30(2):399–414. <https://doi.org/10.1016/j.apt.2018.11.017>.
55. Mourad A, Aissa A, Mebarek-Oudina F, Al-Kouz W, Sahnoun M. Natural convection of nanofluid from elliptic cylinder in wavy enclosure under the effect of uniform magnetic field: numerical investigation. *Eur Phys J Plus*. 2021;136(4):1–18.
56. Vishnu Ganesh N, Al-Mdallal QM, Hirankumar G, Kalaivanan R, Chamkha AJ. Buoyancy-driven convection of MWCNT – Casson nanofluid in a wavy enclosure with a circular barrier and parallel hot/cold fins. *Alex Eng J*. 2022;61(4):3249–64. <https://doi.org/10.1016/j.aej.2021.08.055>.
57. Mourad A, Abderrahmane A, Younis O, Marzouki R, Alazzam A. Numerical simulations of Magnetohydrodynamics natural convection and entropy production in a porous Annulus Bounded by Wavy Cylinder and Koch Snowflake Loaded with Cu-Water Nanofluid. *Micromachines*. 2022;13(2):182.
58. Ma Y, Mohebbi R, Rashidi M, Yang Z, Sheremet MA. Numerical study of MHD nanofluid natural convection in a baffled U-shaped enclosure. *Int J Heat Mass Transf*. 2019;130:123–34.
59. Malekpour A, Karimi N, Mehdizadeh A. Magnetohydrodynamics, natural convection, and entropy generation of CuO-water nanofluid in an I-shape enclosure—a numerical study. *J Thermal Sci Eng Appl*. 2018;10(6):061016.
60. Yadollahi A, Khalesidoost A, Kasaeipoor A, Hatami M, Jing D. Physical investigation on silver-water nanofluid natural convection for an F-shaped cavity under the magnetic field effects. *Eur Phys J Plus*. 2017;132(8):1–13.
61. Raizah ZA, Ahmed SE, Aly AM. ISPH simulations of natural convection flow in E-enclosure filled with a nanofluid including homogeneous/heterogeneous porous media and solid particles. *Int J Heat Mass Transf*. 2020;160: 120153.
62. Abbassi MA, Safaei MR, Djebali R, Guedri K, Zeghmami B, Alrashed AAAA. LBM simulation of free convection in a nanofluid filled incinerator containing a hot block. *Int J Mech Sci*. 2018;144:172–85. <https://doi.org/10.1016/j.ijmecsci.2018.05.031>.

63. Mansour M, Bakier M, Gorla RSR. Natural Convection in Vertical I-Shaped Nanofluid-Filled Enclosures. *J Nanofluids*. 2013;2(3):221–30.
64. Armaghani T, Chamkha A, Rashad AM, Mansour MA. Inclined magneto: convection, internal heat, and entropy generation of nanofluid in an I-shaped cavity saturated with porous media. *J Therm Anal Calorim*. 2020;142(6):2273–85. <https://doi.org/10.1007/s10973-020-09449-6>.
65. Asadi A, Molana M, Ghasemiasl R, Armaghani T, Pop M-I, Safari PM. A new thermal conductivity model and two-phase mixed convection of cuo–water nanofluids in a novel I-shaped porous cavity heated by oriented triangular hot block. *Nanomaterials*. 2020;10(11):2219.
66. Ma Y, Mohebbi R, Rashidi MM, Yang Z, Sheremet M. Nanofluid thermal convection in I-shaped multiple-pipe heat exchanger under magnetic field influence. *Physica A*. 2020;550: 124028. <https://doi.org/10.1016/j.physa.2019.124028>.
67. Abdulkadhim A, Abed IM, Said NM. Magnetohydrodynamics thermogravitational convective in a novel I-shaped wavy-walled enclosure considering various inner hot pipe locations. *J Thermal Anal Calorim*. 2021;29:1–30.
68. Ghasemiasl R, Molana M, Armaghani T, Saffari PM. the effects of hot blocks geometry and particle migration on heat transfer and entropy generation of a Novel I-Shaped porous enclosure. *Sustainability*. 2021;13(13):7190.
69. Biswas N, Manna NK, Datta P, Mahapatra PS. Analysis of heat transfer and pumping power for bottom-heated porous cavity saturated with Cu-water nanofluid. *Powder Technol*. 2018;326:356–69. <https://doi.org/10.1016/j.powtec.2017.12.030>.
70. Chamkha AJ, Ismael MA. Conjugate heat transfer in a porous cavity filled with nanofluids and heated by a triangular thick wall. *Int J Therm Sci*. 2013;67:135–51.
71. Oztop HF, Abu-Nada E. Numerical study of natural convection in partially heated rectangular enclosures filled with nanofluids. *Int J Heat Fluid Flow*. 2008;29(5):1326–36.
72. Sheremet MA, Oztop H, Pop I, Al-Salem K. MHD free convection in a wavy open porous tall cavity filled with nanofluids under an effect of corner heater. *Int J Heat Mass Transf*. 2016;103:955–64.
73. Abdelmalek Z, Tayebi T, Dogonchi A, Chamkha A, Ganji D, Tlili I. Role of various configurations of a wavy circular heater on convective heat transfer within an enclosure filled with nanofluid. *Int Commun Heat Mass Transfer*. 2020;113: 104525.
74. Sheikholeslami M, Gorji-Bandpy M, Ganji D, Soleimani S. Natural convection heat transfer in a cavity with sinusoidal wall filled with CuO–water nanofluid in presence of magnetic field. *J Taiwan Inst Chem Eng*. 2014;45(1):40–9.
75. Motlagh SY, Soltanipour H. Natural convection of Al₂O₃-water nanofluid in an inclined cavity using Buongiorno's two-phase model. *Int J Therm Sci*. 2017;111:310–20. <https://doi.org/10.1016/j.ijthermalsci.2016.08.022>.
76. Kim B, Lee D, Ha M, Yoon H. A numerical study of natural convection in a square enclosure with a circular cylinder at different vertical locations. *Int J Heat Mass Transf*. 2008;51(7–8):1888–906.
77. Nikfar M, Mahmoodi M. Meshless local Petrov-Galerkin analysis of free convection of nanofluid in a cavity with wavy side walls. *Eng Anal Boundary Elem*. 2012;36(3):433–45.
78. Khanafer K, Vafai K, Lightstone M. Buoyancy-driven heat transfer enhancement in a two-dimensional enclosure utilizing nanofluids. *Int J Heat Mass Transf*. 2003;46(19):3639–53.
79. Fusegi T, Hyun JM, Kuwahara K, Farouk B. A numerical study of three-dimensional natural convection in a differentially heated cubical enclosure. *Int J Heat Mass Transf*. 1991;34(6):1543–57.
80. de Vahl DG. Natural convection of air in a square cavity: a bench mark numerical solution. *Int J Numer Meth Fluids*. 1983;3(3):249–64.
81. Barakos G, Mitsoulis E, Assimacopoulos D. Natural convection flow in a square cavity revisited: laminar and turbulent models with wall functions. *Int J Numer Meth Fluids*. 1994;18(7):695–719.

Publisher's Note Springer Nature remains neutral with regard to jurisdictional claims in published maps and institutional affiliations.

Springer Nature or its licensor holds exclusive rights to this article under a publishing agreement with the author(s) or other rightsholder(s); author self-archiving of the accepted manuscript version of this article is solely governed by the terms of such publishing agreement and applicable law.